

PNEUMATIC EXTENSION ACTUATORS WITH KIRIGAMI SKINS

Steven Iannucci and Suyi Li *

Department of Mechanical Engineering
Clemson University, Clemson, SC USA

ABSTRACT

Soft pneumatic actuators have found many applications in robotics and adaptive structures. Traditionally, these actuators are constructed by wrapping layers of reinforcing helical fibers around an elastomeric tube. This approach is versatile and robust, but it suffers from a critical disadvantage: cumbersome fabrication procedures. Wrapping long helical filaments around a cylindrical tube requires expensive equipment or excessive manual labor. To address this issue, we propose a new approach towards designing and constructing pneumatic actuators by exploiting the principle of kirigami, the ancient art of paper cutting. More specifically, we use “kirigami skins”—plastic sleeves with carefully arranged slit cuts—to replace the reinforcing helical fibers. This paper presents an initial investigation on a set of linear extension actuators featuring kirigami skins with a uniform array of cross-shaped, orthogonal cuts. When under internal pressurization, the rectangular-shaped facets defined by these cuts can rotate and induce the desired extension motion. Through extensive experiments, we analyze the elastic and plastic deformations of these kirigami skins alone under tension. The results show strongly nonlinear behaviors involving both in-plane facet rotation and the out-of-plane buckling. Such a deformation pattern offers valuable insights into the actuator’s performance under pressure. Moreover, both the deformation characteristics and actuation performance are “programmable” by tailoring the cut geometry. This study lays down the foundation for constructing more capable kirigami-skinned soft actuators that can achieve sophisticated motions.

Keywords: Kirigami; Pneumatic Actuator; Buckling

1 INTRODUCTION

Soft pneumatic actuators (also referred to as pneumatic artificial muscles) have found many applications in robotic systems as they come in a variety of forms to handle different tasks like gripping [1–3], bending [4–6], and linear extension [7]. Traditionally, these actuators are constructed by wrapping long helical fibers around an elastomeric tube. They are light-weight and safe to operate with humans. Moreover, their performance is highly tailorable by carefully designing the underlying helical fiber geometries [8–11]. However, the fabrication of these fiber-reinforced actuators is a lengthy and expensive process, either requiring expensive equipment (e.g., filaments winding or braiding machine) or much manual labor (e.g., manual fiber wrapping with the help of 3D printed molds [10, 11]). Such fabrication complexity also leads to inevitable uncertainty in the actuators’ performance.

To address these issues, we propose the concept of using “kirigami skins” for the pneumatic actuator as a method to produce programmable actuation performance with less manufacturing effort (Figure 1, 2). Kirigami, the ancient art of paper cutting, has become a popular research subject recently due to its unique properties along with relative ease of manufacturing. With the addition of carefully designed cuts, a thin sheet can become a sophisticated 3D shape by stretching, folding, or other manipulation techniques. Given that cutting is scalable, kirigami principles have found applications in many engineered systems with vastly different scales, like composite laminates [12, 13], nano/mesoscale structures [14–18], and robotics [19–21]. In particular, one can combine kirigami wrapping with other linear soft actuators to improve the performance of crawling robots, especially increasing the friction force with the ground [20, 22–24].

* Address all correspondence to this author: suyil@clemson.edu.

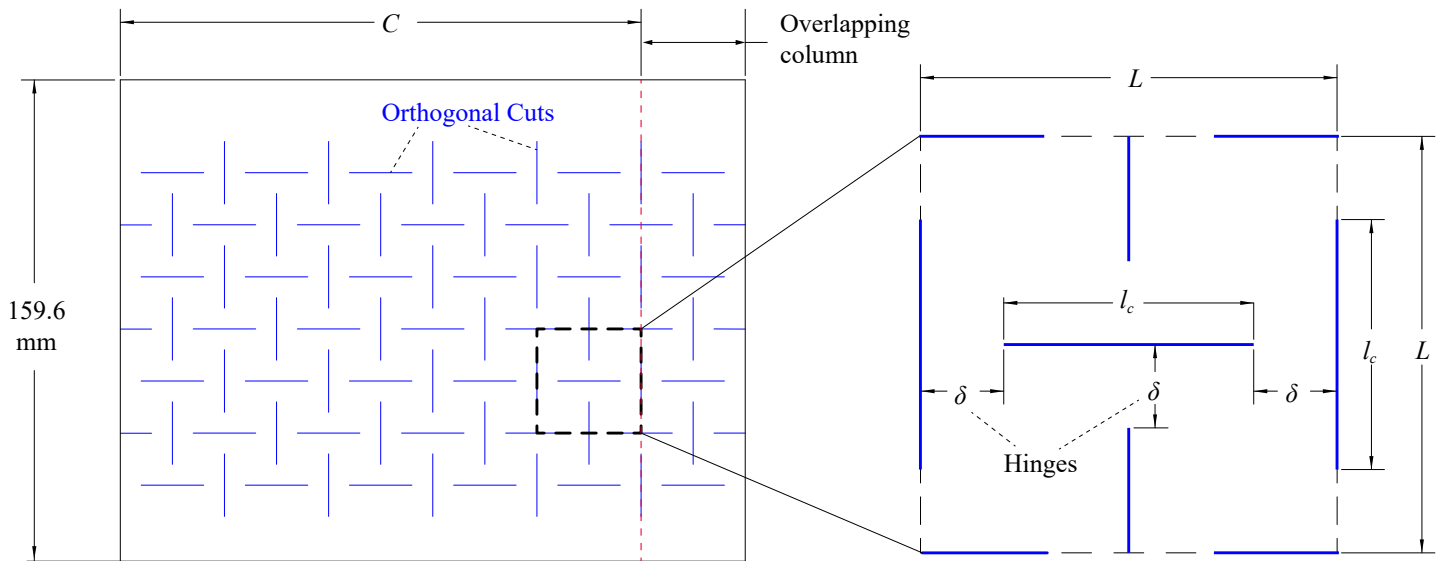


FIGURE 1. An example of kirigami skin design: Here, a single element is scaled up to show the geometry of the cuts (shown by solid blue lines) made in the sheet material. The hinges between cuts are shown as δ . The column of elements to the right of the red dashed line is for overlapping during assembly.

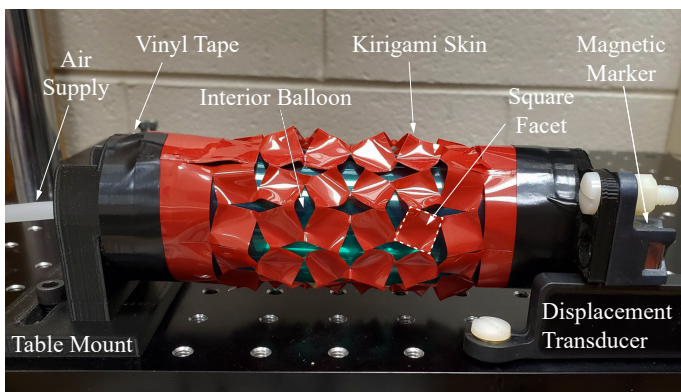


FIGURE 2. A kirigami-skinned soft pneumatic actuator under internal pressure, showing the linear extension motion.

In this study, we propose creating kirigami skins with an array of mutually orthogonal cuts to deform non-uniformly and obtain a linear actuation. These kirigami skins are fabricated by using a plotter cutter or laser cutter, which is more precise, efficient, and cost-effective than the reinforcing fiber wrapping methods. When under internal pressurization, the rectangular-shaped facets defined by the orthogonal cuts can rotate and induce extension motion. Therefore, the objective of this study is to understand how the design and mechanical properties of Kirigami skins influence the actuator performance. To this end, we first examine the elastic and plastic deformation of the

Kirigami skin *alone* under axial tension by comprehensive experimental tests. Our results show a three-phase deformation cycle in which a strongly nonlinear response is present. The second deformation region, defined by both in-place rotation and out of plane buckling of the facet, is where the majority of extension occurs. Then, we examine the performance of the kirigami skinned actuator under internal pressure. We find that the actuator free-stroke is also strongly nonlinear, and correlates directly to the skin deformation pattern under tension. Moreover, both the deformation characteristics and actuation performance are “programmable” by tailoring the cut geometry.

In what follows, Section 2 briefly describes the design of Kirigami skin. Section 3 and 4 detail the experimental study on the Kirigami skin deformation and the overall actuator performance, respectively. Section 5 ends this paper with a summary and conclusion.

2 Design Of The Kirigami Skin

A kirigami skin in this study has periodically distributed and mutually orthogonal cuts that divide the sheet into an array of repeating elements (Figure 1). Each element can be described by a few design parameters, including the element size L , slit cut length l_c within the element, and the “hinge” size δ between the cuts. In this study, we fix the total length C of the kirigami skin because it is supposed to wrap around a cylindrical fitting of 50.8mm diameter (aka. $C = \pi d_0 = 159.6\text{mm}$). So the element size L is related to the total number of elements N along

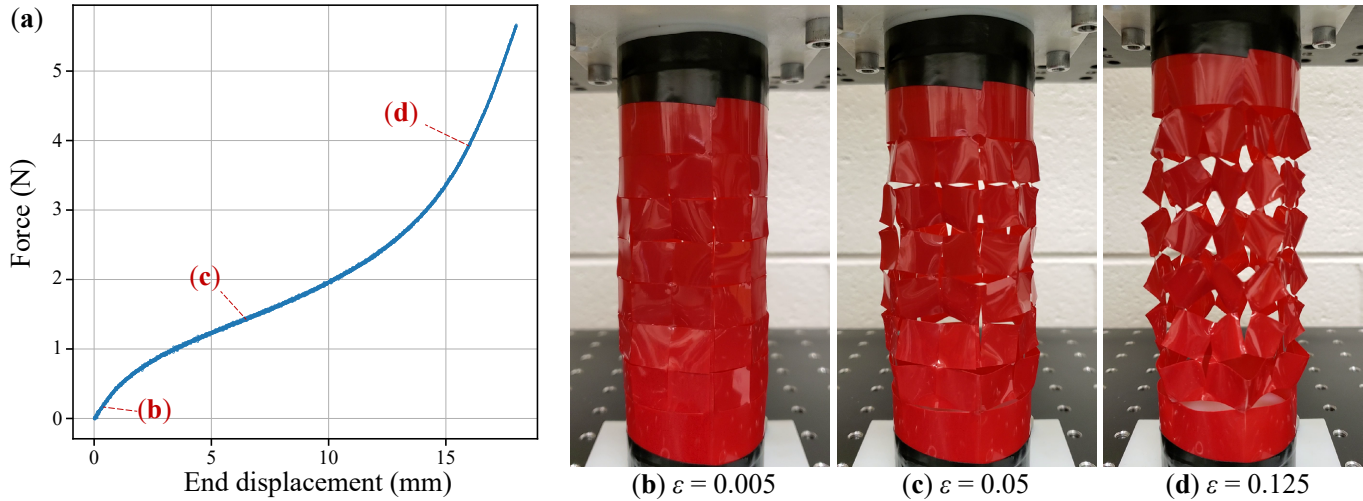


FIGURE 3. Deformation pattern of a sample Kirigami skin with $N = 6$ and $R = 6$. a): The force-displacement curve, notice that only the extension responses are shown here. The three different phases of deformation are highlighted at $\varepsilon = 0.005$, 0.05 , 0.125 . (b, c, and d): The external shapes of the skin at the noted strain levels.

the length of kirigami skin according to Equation 1. The total height of a kirigami skin is set at 127.0mm.

$$L = \frac{C}{N} = 2\delta + l_c. \quad (1)$$

Besides the number of elements N along the skin length, we define another independent design variable R as the ratio of the slit cut length over hinge size in that

$$R = \frac{l_c}{2\delta}. \quad (2)$$

As R increases, the cut becomes relatively longer, leaving smaller hinges to connect the square facets. To ensure reliable actuation performance, we add an extra column of elements and overlap this column to the one on the other side of the kirigami skin when we wrap it around the interior balloon. Without this overlapping, the kirigami skin would have a discontinuous break, causing the inner tube to bulge through under pressure.

In what follows, we show how that the kirigami skins can effectively constrain an inflatable balloon and transform its volumetric expansion into extension, and how adjusting the two independent design parameters (aka. element number N and cut ratio R) can create a broad spectrum of skin deformation pattern and actuator performance.

3 Deformation of Kirigami Skins Under Tension

We first analyze the deformation characteristics of the kirigami skin *alone* by uniaxial tensile testing, because the kirigami deformation under this loading condition is directly related to the actuation performance. We first use an FCX4000 plotter (Graphtec, Tokyo, Japan) to cut an array of perpendicular slits in a 0.5mm thin Artus Plastic Shim Stock. These kirigami skins are connected to two 3D printed fittings via double-sided tape, and each fitting has a diameter of 50.8 mm and a height of 25.4 mm. The overlapping column of kirigami elements is also secured with thin, double-sided tape to create a cylindrical-shaped skin with a uniform cut pattern. Also, vinyl tapes are wrapped around the exterior of the skin and mount to ensure fixed end conditions. Finally, we secure the assembly to an eXpert 5061 universal tester machine with an 25 lb load cell (ADMET, Norwood MA, Figure 3).

For the tensile tests, we first stretch the kirigami skin samples to an initial deformation at a rate of 0.5 mm/s and then cycle back to the starting position. After completing three initial stretching cycles, we increase the tensile deformation by 2 mm in every subsequent stretch.

We fabricated and tested 24 kirigami skin samples with unique cutting pattern designs. The samples have ($N =$) 6, 8, 10, or 12 elements in the circumferential direction (or length direction of the unwrapped flat Kirigami sheet). The cut ratio R defined in Equation 2 is varied from 2 to 7 for each N value.

Deformation Phases Figure 3(a) displays the force-end displacement relationship of a kirigami skin ($N = 6$, $R = 6$) during extension, from which one can observe three distinct phases.

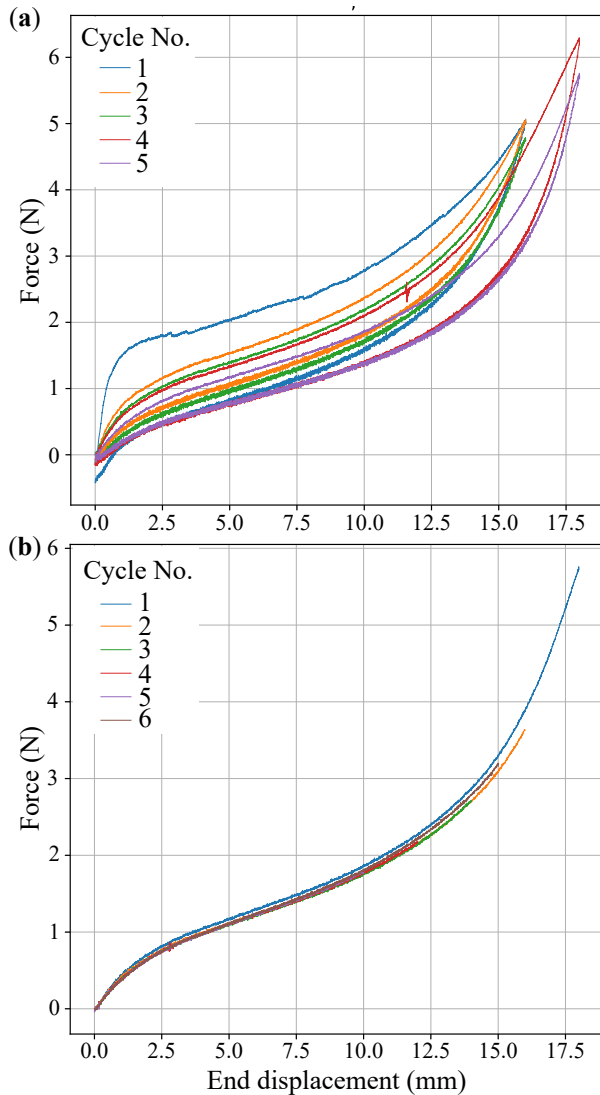


FIGURE 4. Plastic deformation of the kirigami skin under stretch. (a) The force-displacement curves of a sample, $N = 6$ and $R = 6$. Three cycles to 16 mm of displacement and two cycles of 18 mm of displacement are presented. (b) The force-displacement curves of a sample during elongation. The sample was stretched to 18 mm to start, and then stretched 2mm less in the subsequent cycles. Notice that only the stretching part of load cycles are shown here for clarity

At small end displacements (or small strain ϵ), the response of kirigami skin is relatively linear without any significant deformations (Figure 3(b)). As the end displacement increases to a critical threshold, kirigami skin deformation enters its second phase as its square facets began to rotate and deform out-of-plane. As a result, the slit cuts begin to open (Figure 3(c)). These out-of-plane deformations seem non-uniform and random initially. However, as the end displacement gradually increases, the square

facets start to “snap” and align with each other, and the hinges between the facets start to buckle (shown by the small drops in the reaction force curve) until they all settle into the final deformation pattern (Figure 3(d)). In this final pattern, every square facet rotates oppositely to its adjacent neighbors, and the slit cuts become rhomboid-shaped gaps. Once reaching this final deformation pattern, the kirigami skin enters the third phase of deformation, where the skin deforms mainly at its hinges. It is worth noting the cylindrical kirigami skin is not as stretchable as a unwrapped flat kirigami sheet with the same cutting pattern design, because there are additional deformation compatibility constraints in the circumferential direction.

Plasticity The plastic deformation of the hinges plays an essential role in the nonlinear response of kirigami skin. Figure 4 shows the force-deformation relationship of two skin samples with the same cutting pattern design ($N = 6$, $R = 6$) but different loading sequences. For the first sample, we stretch it with a 16mm end displacement for the first three loading cycles and then increase the end displacement to 18mm in the next two cycles. For the second sample, we stretch it with an 18mm end displacement in the first loading cycle, and then reduce the end displacement by 2 mm in every subsequent cycle. In different loading cycles, we observe different force-displacement curves during the stretch, as well as energy loss and hysteresis due to plastic deformation in the hinges. The force-displacement curve and hysteresis magnitudes vary significantly depending on the loading history. First, if the total end displacement does not change, the kirigami skin becomes softer and provides less resistance to the extension after every loading cycle, and its hysteresis also reduces (e.g., from cycle 1 to 3, or from cycle 4 to 5 in Figure 4(a)). These changes are probably because the hinges become predisposed (or preconditioned) to the out-of-place buckling. However, if we stretch the kirigami skin with a new end displacement that it has never experienced before (e.g., from cycle 3 to 4 in Figure 4(a)), we can observe a jump in resistance and hysteresis. Secondly, if we stretch the kirigami skin with a maximum end displacement without failure (e.g., cycle 1 in 4(b)), the skin shows a consistent force-displacement curve *during extension* in the subsequent loading cycles that have smaller end displacements (e.g., cycle 2 to 5 in 4(b)). Such consistency in the nonlinear responses comes from the fact that the hinges in the kirigami sheet have been plastically deformed as much as possible without failure, so no new plastic deformation can occur in the following load cycles.

Parametric Analyses Finally, we observe that the two independent kirigami design parameters (N , R) have a strong influence on the overall nonlinear responses. The cut ratio of R relates to the maximum strain achievable by the kirigami skin samples (Figure 5(a)). Our samples with the largest hinge size

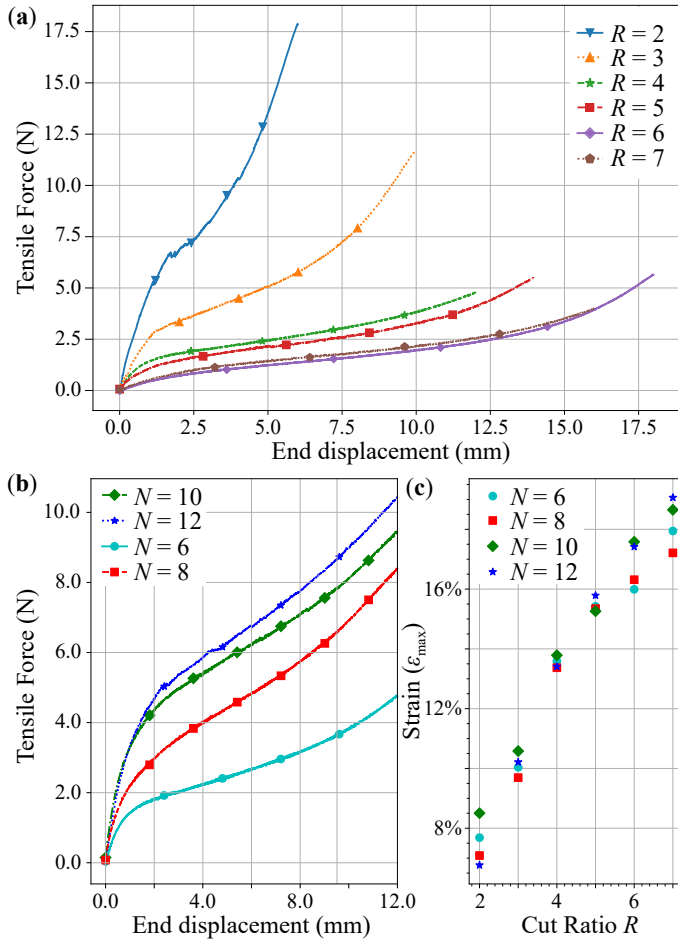


FIGURE 5. Correlations between stretch response and cutting designs of the Kirigami skin. (a): Comparing the force-displacement curves of kirigami skin samples with the same element number $N = 6$ but different cut ratios. (b) Comparing the force-displacement curves of samples with the same cut ratio $R = 4$ but different element numbers. Again, only the stretching part of loading cycles are shown here for clarity. (c) The maximum strain of each sample at failure.

or shortest slit cuts ($R = 2$) can withstand much higher tensile forces, yet fail at significantly lower strains. The large hinge size in these samples prevents the slit cuts from opening significantly and causing the skin to enter the third phase of nonlinear responses at a smaller stretch. On the other hand, kirigami skins with the smallest hinge size or the longest slit cuts ($R = 6, 7$) allows for a more elongation with less reaction force. The square facets in these samples can rotate by the largest angle possible according to the kinematic constrain. Finally, the maximum stretch at failure increases significantly as R increases (Figure 5(c)).

The number of elements in the kirigami skin (N) relates to the magnitude of the reaction force at a given stretch. Generally speaking, skins with smaller N , or large elements size, give lower

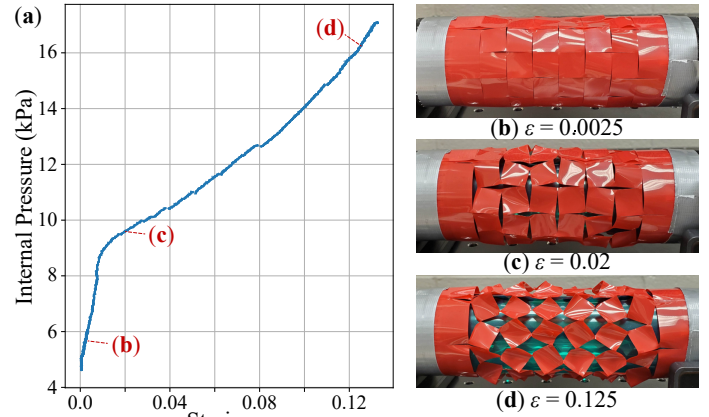


FIGURE 6. Linear extension actuator with a Kirigami skin of $N = 6$ and $R = 6$. (a): The pressure-stroke relationship of this actuator. Notice that only the pressuring phase is shown here for clarity. The different phases of deformation are highlighted at $\epsilon = 0.0025, 0.02$, and 0.125 . (b, c, and d) The actuator deformation at these strain levels.

resistance force. Moreover, the element size does not seem to affect the maximum stretch at failure (Figure 5(b, c)).

4 Pneumatic Actuation Performance

The deformation patterns of the kirigami skin alone under stretch, as well as its correlation to the cut pattern design, can directly inform the pneumatic actuator performance. In this section, we show that 1) the kirigami skin, once being wrapped around an inflatable balloon, is capable of transforming the volumetric expansion into an extension actuation, and 2) it is feasible to fine-tune the actuation performance by adjusting underlying kirigami design parameters.

We use 50mm diameter balloons (Qualatex, North Wichita, KS) to contains the pneumatic pressure. Each balloon, with an initial length of about 40mm, is connected to 3D-printed end caps and inflated to the length of the undeformed kirigami skin before testing. The kirigami skin is attached to the end caps using double-sided tack film and wrapped around the caps and interior balloon. Again, we secure an overlapping column of elements using a double-sided tack film and then wrap vinyl tape outside of the skin-end cap assembly for extra support (Figure 2).

To measure the free stroke of these actuators, we mount one of the actuator end caps to a non-ferrous bed while leaving the other end cap free. A non-contact electromagnetic linear displacement transducer (SPS-L075-HALS, Honeywell, Charlotte, NC) was mounted to the bed, with the magnetic positional marker secured to the free-moving end cap (Figure 2).

Pneumatic pressure is supplied using a solenoid valve (ControlAir 900X, Amherst, NH) and measured by a gauge pressure sensor (SSCDANN005PGAA5, Honeywell, Charlotte, NC).

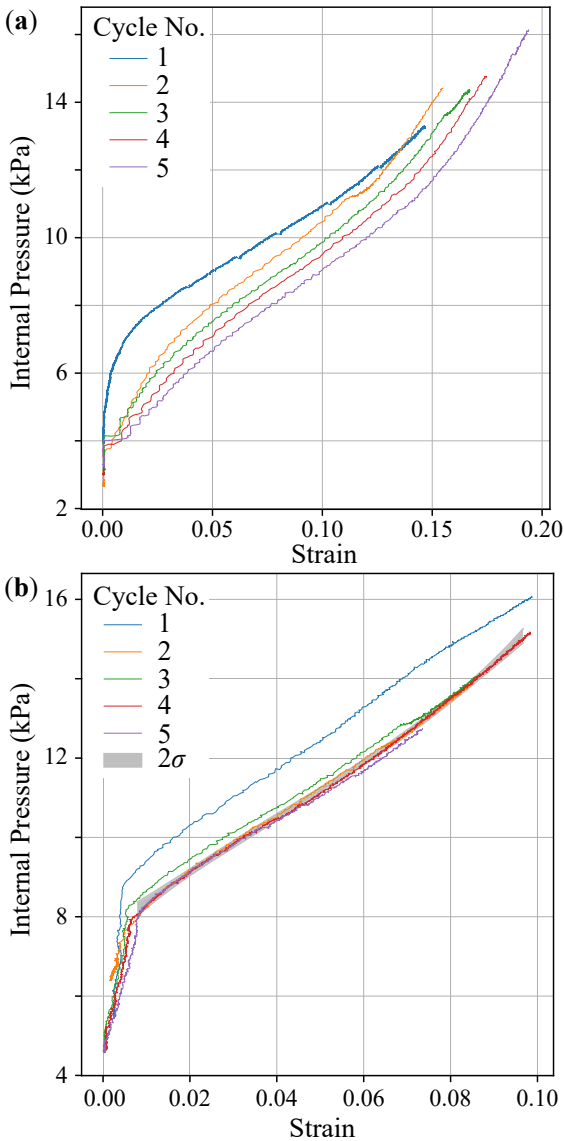


FIGURE 7. The influences of plastic deformation on actuator performance. (a): The actuation performance of a sample with $N = 10$ and $R = 7$. Five pressurization tests are presented, where each test reaches a larger maximum stroke than the previous one. (b) The performance of a pre-conditioned actuator with $N = 8$ and $R = 5$. This sample was pressurized to achieve a maximum 10% stroke first. In the following tests, the actuator operates with lower strokes and shows consistent and repeatable performance. For clarity, only the pressurization part of the actuation cycles are presented here.

Once the actuator reaches full extension, we release the pressure by a manual relief push-button valve, which returns the actuator to its initial length. The pressure sensor and displacement transducer readings are linked using LabView via an analog data

acquisition instrument (National Instruments, Austin, TX).

Phases of Actuation In the actuation tests, the kirigami skins show similar deformation patterns to those observed in the uniaxial tensile tests. Figure 6(a) displays the pressure-stroke curve of an actuator during its pressurization phase. Initially, the kirigami skin shows minimal deformation at low pressure (Figure 6(b)), and this stage directly relates to the first phase of the skin stretch tests shown in Figure 3. Once the pressure reaches a critical value, the square facets in the kirigami skin begin to rotate, and the hinges start to buckle out-of-plane as displayed in Figure 6(c). However, due to the contact force from the interior balloon, we do not observe the random “snaps” that are evident in the skin stretch tests. As the pressure continues to increase, the square facets in the kirigami skin rotate towards the maximum possible angle allowed by the kinematic constraints.

On the hand, the Kirigami skin deformation in the actuator test start to differ from the tension test as the stroke becomes high. Figure 6(d) shows the actuator close to its maximum stroke. At this stage, the balloon has fully expanded and filled the entire volume enclosed by the kirigami skin. It pushes the kirigami skin from inside and constrains the skin deformation. As a result, we do not observe a significant third phase, as seen in the skin stretch tests in Figure 3, especially when the cut ratio is relatively small.

Plasticity The kirigami skin shows a similar plastic behavior to those observed in the skin tensile tests. That is, the response of the skin during pressurization depends on the maximum strain previously achieved by this sample. Figure 7(a) shows the response of an actuator sample over five pressurization cycles. In each cycle, we increase the pressure until this actuator reaches a new maximum stroke that it has not achieved before. Due to the progressively increasing plastic deformations in the hinges, the kirigami skin shows less resistance against pressure over the loading cycles, thus providing better performance in terms of the free stroke at a given pressure. Therefore, in order to create an actuator with consistent performance over many pressurization cycles, the kirigami actuator must be pressurized to its maximum strain without failure as a pre-conditioning procedure before practical implementation. Figure 7(b) presents the performance of an actuator sample that is pre-conditioned by a maximum free stroke of 10% (pressurization cycle 1). Once this pre-condition is complete, the actuator operates with a lower stroke and shows reliable repeatability.

Parametric Analyses Similar to the skin stretching test, actuation performance of the kirigami actuator is closely related to the underlying cutting pattern design. For example, a larger cut ratio of R in the kirigami skin gives a greater maximum free stroke (Figure 8(a)). This is because the smaller hinges corre-

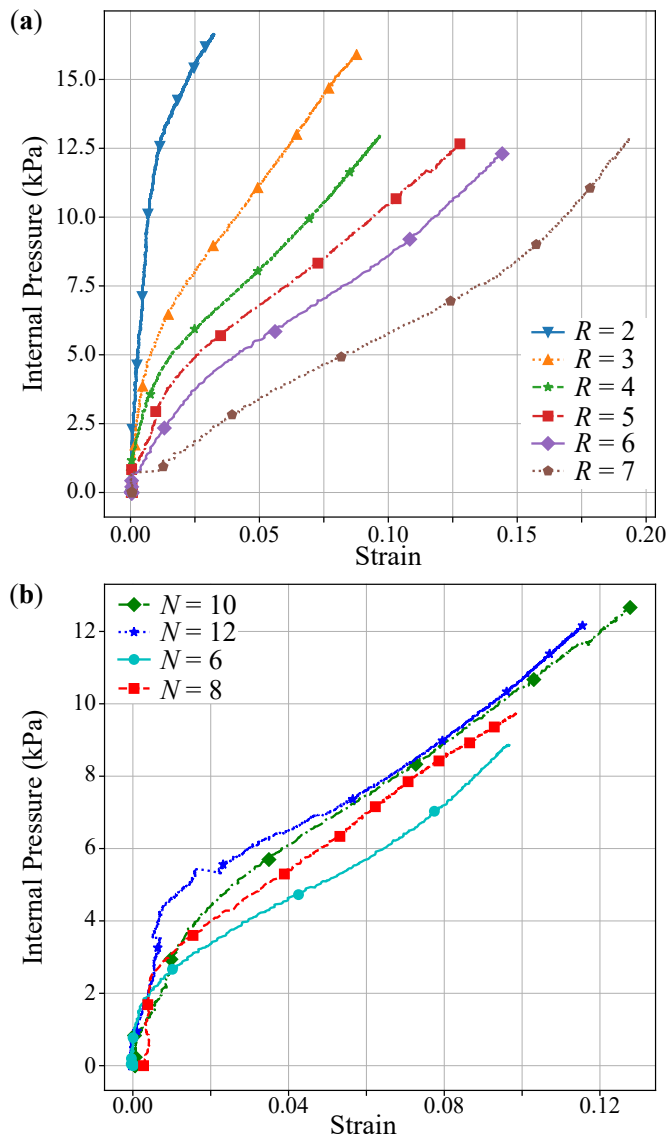


FIGURE 8. The correlations between the actuator performance and underlying Kirigami designs. (a) Comparing the pressurization response of various samples with the same element number $N = 10$ but different cut ratios. (b) Comparing the response of samples with the same cut ratio $R = 5$ but different element numbers.

sponding to the high cut ratio can rotate to a greater opening angle. In our test, we are able to achieve close to 20% of free stroke with $R = 7$. On the other hand, kirigami skins with a smaller cut ratio (or large hinge size) can withstand higher internal pressure. The number of elements in the kirigami skin, on the other hand, has a limited effect on the actuation performance (Figure 8(b)). Generally speaking, a kirigami skin with more elements requires more pressure to reach the same free stroke.

5 Summary and Conclusion

In this study, we propose and examine the concept of soft pneumatic actuators with kirigami skins defined by an array of mutually orthogonal cuts. These slit cuts allow for the skin to deform non-uniformly and convert the internal pressure into linear motion. To understand the mechanics of these cylindrical kirigami skins under tension and its correlation to pneumatic actuation performance, we first tested skin samples *alone* in uniaxial tension. The behaviors of these skin can be described as three-phase deformation cycles in response to stretching. Importantly, the second deformation phases are defined by the in-plane rotation of the square facets and out-of-plane buckling of hinges, generating a nonlinear extension curve. Then, we wrap the kirigami skins around an inflatable balloon to create linear actuators. The skins proved to be an effective mechanism to convert internal pressure into linear motion, showing a similar deformation pattern as these observed in the tensile tests.

The kirigami skin performs well as a mechanism that transforms the pressure-driven volumetric expansion into a linear actuator extension. Moreover, one can prescribe the actuation performance in terms of free stroke by fine-tuning the underlying kirigami cutting pattern design according to the specific application requirements. For reliable and repeatable actuation performance, each kirigami skin should be pre-conditioned by being stretched to its maximum length without failure before being used. Moreover, the actuator can remain pressurized sufficiently so that the skin never exits the second deformation phase, offering a nearly linear correlation between internal pressure rise and free stroke. The results of this paper pave the foundation for establishing a design and analysis framework for constructing kirigami-skinned pneumatic actuators with sophisticated actuation capability.

ACKNOWLEDGMENT

The authors acknowledge the support from Clemson University (via startup fund and CECAS Dean's Faculty Fellow Award) and National Science Foundation (CMMI-1751449 CAREER, 1760943, and 1933124).

REFERENCES

- [1] Rodrigue, H., Wang, W., Kim, D. R., and Ahn, S. H., 2017. "Curved shape memory alloy-based soft actuators and application to soft gripper". *Composite Structures*, **176**, pp. 398–406.
- [2] Wang, T., Zhang, Y., Zhu, Y., and Zhu, S., 2019. "A computationally efficient dynamical model of fluidic soft actuators and its experimental verification". *Mechatronics*, **58**(October 2018), pp. 1–8.
- [3] Zhou, X., Majidi, C., and O'Reilly, O. M., 2015. "Soft hands: An analysis of some gripping mechanisms in soft

- robot design”. *International Journal of Solids and Structures*, **64**, pp. 155–165.
- [4] Singh, G., Xiao, C., Hsiao-Weckler, E. T., and Krishnan, G., 2018. “Design and analysis of coiled fiber reinforced soft pneumatic actuator”. *Bioinspiration and Biomimetics*, **13**(3).
- [5] Polygerinos, P., Wang, Z., Overvelde, J. T., Galloway, K. C., Wood, R. J., Bertoldi, K., and Walsh, C. J., 2015. “Modeling of Soft Fiber-Reinforced Bending Actuators”. *IEEE Transactions on Robotics*, **31**(3), pp. 778–789.
- [6] Darmohammadi, A., Naeimi, H. R., and Agheli, M., 2018. “Effect of fiber angle variation on bending behavior of semi-cylindrical fiber-reinforced soft actuator”. *Proceedings of the ASME Design Engineering Technical Conference*, **5B-2018**, pp. 1–6.
- [7] Cho, K. H., Song, M. G., Jung, H., Yang, S. Y., Rodrigue, H., Moon, H., Koo, J. C., and Choi, H. R., 2017. “Biomimetic robotic joint mechanism driven by soft linear actuators”. *Proceedings - IEEE International Conference on Robotics and Automation*, pp. 1850–1855.
- [8] Geer, R., Iannucci, S., and Li, S., 2020. “Pneumatic Coiling Actuator Inspired by the Awns of *Erodium cicutarium*”. *Frontiers in Robotics and AI*, **7**.
- [9] Wang, Y., and Xu, Q., 2018. “Design and Fabrication of a Soft Robotic Manipulator Driven by Fiber-Reinforced Actuators”. *2018 IEEE International Conference on Mechatronics, Robotics and Automation, ICMRA 2018*, pp. 157–161.
- [10] Iida, F., and Laschi, C., 2011. “Soft robotics: Challenges and perspectives”. *Procedia Computer Science*, **7**, pp. 99–102.
- [11] Isobe, M., Okumura, K., Kim, T., Lee, Y. G., Kim, S., Laschi, C., Trimmer, B., Polygerinos, P., Wang, Z., Overvelde, J. T., Galloway, K. C., Wood, R. J., Bertoldi, K., Walsh, C. J., Connolly, F., Walsh, C. J., Bertoldi, K., Rossiter, J., Sareh, S., Dias, M. A., McCarron, M. P., Rayneau-Kirkhope, D., Hanakata, P. Z., Campbell, D. K., Park, H. S., Holmes, D. P., Polygerinos, P., Wang, Z., Overvelde, J. T., Galloway, K. C., Wood, R. J., Bertoldi, K., Walsh, C. J., Rafsanjani, A., Jin, L., Deng, B., Bertoldi, K., and Jamalzadeh, M., 2017. “Modeling of Soft Fiber-Reinforced Bending Actuators”. *Proceedings of the National Academy of Sciences of the United States of America*, **31**(3), pp. 778–789.
- [12] Cui, J., Poblete, F. R., and Zhu, Y., 2018. “Origami/Kirigami-Guided Morphing of Composite Sheets”. *Advanced Functional Materials*, **28**(44), pp. 1–7.
- [13] Lele, A., Deshpande, V., Myers, O., and Li, S., 2019. “Snap-through and stiffness adaptation of a multi-stable Kirigami composite module”. *Composites Science and Technology*, **182**(July), p. 107750.
- [14] Cai, K., Luo, J., Ling, Y., Wan, J., and Qin, Q. H., 2016. “Effects of size and surface on the auxetic behaviour of monolayer graphene kirigami”. *Scientific Reports*.
- [15] Zhang, Y., Yan, Z., Nan, K., Xiao, D., Liu, Y., Luan, H., Fu, H., Wang, X., Yang, Q., Wang, J., Ren, W., Si, H., Liu, F., Yang, L., Li, H., Wang, J., Guo, X., Luo, H., Wang, L., Huang, Y., and Rogers, J. A., 2015. “A mechanically driven form of Kirigami as a route to 3D mesostructures in micro/nanomembranes”. *Proceedings of the National Academy of Sciences of the United States of America*, **112**(38), pp. 11757–11764.
- [16] Yan, Z., Zhang, F., Wang, J., Liu, F., Guo, X., Nan, K., Lin, Q., Gao, M., Xiao, D., Shi, Y., Qiu, Y., Luan, H., Kim, J. H., Wang, Y., Luo, H., Han, M., Huang, Y., Zhang, Y., and Rogers, J. A., 2016. “Controlled Mechanical Buckling for Origami-Inspired Construction of 3D Microstructures in Advanced Materials”. *Advanced Functional Materials*, **26**(16), pp. 2629–2639.
- [17] Firouzeh, A., Higashisaka, T., Nagato, K., Cho, K., and Paik, J., 2020. “Stretchable kirigami components for composite meso-scale robots”. *IEEE Robotics and Automation Letters*, **5**(2), pp. 1883–1890.
- [18] Cheng, Y. C., Lu, H. C., Lee, X., Zeng, H., and Primagi, A., 2020. “Kirigami-Based Light-Induced Shape-Morphing and Locomotion”. *Advanced Materials*, **32**(7).
- [19] Rossiter, J., and Sareh, S., 2014. “Kirigami design and fabrication for biomimetic robotics”. *Bioinspiration, Biomimetics, and Bioreplication 2014*, **9055**(March 2014), p. 90550G.
- [20] Rafsanjani, A., Zhang, Y., Liu, B., Rubinstein, S. M., and Bertoldi, K., 2018. “Kirigami skins make a simple soft actuator crawl”. *Science Robotics*, **3**(15).
- [21] Qiu, C., Dai, J. S., and Qiu, C., 2015. “Helical Kirigami-Enabled Centimeter-Scale Worm Robot With Shape-Memory-Alloy Linear Actuators Helical Kirigami-Enabled Centimeter-Scale Worm Robot With Shape-Memory-Alloy Linear Actuators screw system”. pp. 1–10.
- [22] Rafsanjani, A., Jin, L., Deng, B., and Bertoldi, K., 2019. “Propagation of pop ups in kirigami shells”. *Proceedings of the National Academy of Sciences of the United States of America*, **116**(17), pp. 8200–8205.
- [23] Branyan, C., Hatton, R. L., and Menguc, Y., 2020. “Snake-inspired kirigami skin for lateral undulation of a soft snake robot”. *IEEE Robotics and Automation Letters*, **5**(2), pp. 1728–1733.
- [24] Sedal, A., Memar, A. H., Liu, T., Menguc, Y., and Corson, N., 2020. “Design of Deployable Soft Robots through Plastic Deformation of Kirigami Structures”. *IEEE Robotics and Automation Letters*, **5**(2), pp. 2272–2279.